Hydrogen-Bonded Clusters on the Vapor/Ethanol-Aqueous-Solution Interface

Yoshimichi Andoh* and Kenji Yasuoka

Department of Mechanical Engineering, Keio University, 3-14-1 Hiyoshi, Kohoku-ku, Yokohama 223-8522, Japan

Received: February 23, 2006; In Final Form: August 17, 2006

The structure of the vapor/ethanol-aqueous-solution interface has been carefully investigated focusing on an intermolecular hydrogen bond (HB) and molecular clusters bound by HBs. This paper is a continuation of our previous molecular dynamics (MD) study (*Langmuir* **2005**, *21*, 10885), and all analysis was performed based on five independent adsorption-equilibrated configurations of a slab of ethanol solution at 298.15 K, where the ethanol mole fraction of the solution, χ_e, is 0.0052, 0.012, 0.024, 0.057, and 0.12, respectively. The geometrical definition of HB enabled the detection of the HB between ethanol−ethanol, ethanol−water, and water−water molecules. The variations of the density of HB and the coordination number of HB across the vapor/solution interface were analyzed. Analysis on the density of HB reveals that a monolayer of adsorbed ethanol can be classified into two parts where ethanol molecules prefer to form HBs with each other and ethanol molecules prefer to form HBs with water molecules. Despite χ_e, the coordination number of ethanol−ethanol HB monotonically increases toward the vapor region, while those of ethanol−water and water−water HBs monotonically decrease. In addition, the variation of the mean size of both ethanol one-component clusters and ethanol/water binary clusters across the interface were analyzed. The mean size of an ethanol one-component cluster and that of an ethanol/water binary cluster are expressed as a maximum at the interface. These behaviors are linked with the size distributions of both one-component and binary clusters. A relatively large system in this calculation also enables detailed discussion about the molar dependency of the bulk structural properties of an ethanol solution.

1. Introduction

Alcohol aqueous solutions play an important role in both scientific and technological fields. They are regarded as an elementary system composed of a mixture of soluble amphiphilic surfactant and water. Thus far, interest has mainly focused on their nonideal (excess) behavior regarding thermophysical properties. It is assumed that the origin of these nonideal properties is related to the molecular structure of the solution. A large number of experimental studies,[1−9] theoretical studies,[10−13] and molecular simulation studies[14−22] have been carried out in alcohol/water mixtures, focusing on the structure of the molecular cluster due to hydrogen bond (HB). In such studies, ethanol (C_2H_5OH) aqueous solutions, as well as methanol (CH_3OH) solutions, have been frequently selected as test mixtures due to the structural simplicity of the alcohol molecule.

The clustering of ethanol molecules in a bulk aqueous solution is experimentally investigated by the Kirkwood−Buff parameter.[1−4] The rapid increase of the ethanol−ethanol Kirkwood−Buff parameter with ethanol mole fraction χ_e in a dilute region ($\chi_e < 0.15$) indicates that the clustering of ethanol molecules is enhanced with χ_e. Nishi et al. clarified the detail of the binary clustering of ethanol and water molecules by the combination of infrared spectroscopy (IR), mass spectroscopy (MS), and X-ray diffraction at 308 K.[7,8] The result of IR spectroscopy showed that there exist tiny amounts of ethanol dimers even in a very diluted aqueous solution ($\chi_e \sim 0.001$). The result of MS indicated that the ratio of number of water molecules to ethanol molecules in an ethanol/water binary cluster is 2 ± 1 when $\chi_e = 0.02$. It is then suggested that the binary cluster contains a hydrophobic core structure composed of coherent ethyl groups of ethanol molecules surrounded by a strong water hydrogen-bonding cage. Consequently, Wakisaka and Ohki carried out a series of MS studies on primary alcohol aqueous solutions (methanol, ethanol, and 1-propanol).[9] It is suggested that the hydrogen-bonding network of water is not influenced by the presence of ethanol when χ_e is low and that an incorporation of ethanol molecules into the binary cluster are achieved by substitution of a water molecule. This molecular picture of the binary cluster may not be consistent with that of Nishi et al. because the formation of an ethanol core is not necessarily assumed.

Molecular simulations, such as molecular dynamics (MD) and Monte Carlo (MC) simulations, provide more direct insight on the clustering of alcohol molecules in aqueous solution. A methanol aqueous solution is most frequently investigated,[14−18,21] followed by ethanol,[19,21] 1-propanol,[20,21] 1-butanol,[21] and *tert*-butyl alcohol aqueous solutions.[22] Essentially, these MD works reported that alcohol and water molecules are not ideally mixed at the molecular level despite miscibility (or partial miscibility) of both components. Even in a water-rich region, alcohol molecules tend to form one-component clusters.[16,18,20,22] For example, Dixit et al. reported that, in a dilute solution of methanol (methanol mole fraction $\chi_m = 0.05$), more than 80% of methanol forms one-component clusters with a size of 3−8, where intermolecular connections are simply defined by the position of the first minimum of the C−C pair distribution function.[16] It is also revealed that lengthening of the hydrocarbon chain induces the self-association of alcohol molecules in a micelle-like shape in which intervenient water molecules bridge

* Corresponding author. E-mail: yandoh@ims.ac.jp.

10.1021/jp061150k CCC: $33.50
Published on Web 11/02/2006

a gap between linear alcohol clusters.[20] To our knowledge, however, there has not been a series of MD investigations on the variation of molecular clustering in an ethanol aqueous solution with χ_e.

In contrast, the interfacial properties become more important when alcohol aqueous solution are applied to a technological field. The vapor/solution interface is the main location where reactants in the gas phase solvate into solution or reactants in the bulk solution adsorb. To control the rate of the reaction, it is undoubtedly significant to understand these processes at a moleculer level. Until now, many kinds of experimental studies, such as neutron and X-ray reflection,[23,24] sum−frequency vibrational spectroscopy,[25−27] and surface excess entropy measurements,[28,29] have been done, partially revealing the molecular structure of the vapor/alcohol-aqueous-solution interface. It can be stated, however, that the extent of the understanding of the interfacial molecular structure is insufficient for constructing a picture of the processes describing gas solvation and solute adsorption.

Molecular simulations have shown great potential in providing direct information about the molecular structure of the vapor/alcohol-aqueous-solution interface.[30−33] In the pioneering work by Matsumoto et al. on the vapor/methanol-aqueous-solution interface,[30] it is revealed that both methanol and water molecules have preferable orientations at the interface. The interface of the vapor/ethanol-aqueous-solution was first investigated by Tarek et al.,[31] where the local structure of the solution at the interface was illuminated in terms of intermolecular HB. They found that the state of the HB of an ethanol molecule at the interface is much different from that in the bulk solution, mainly because of the preferential orientation of ethanol molecules at the interface. Stewart et al. carried out a more detailed investigation on the local structure of the solution.[32] They reported the coordination number of HB with the classification of the role of acceptor/donor, contrasting the results in the bulk region with that at the interface. The remaining problem is to elucidate how the ethanol molecule aggregates at the interface and how the state of the aggregates (i.e., clusters) differs when compared with that in the bulk solution.

We have recently carried out a MD study where the two-dimensional "phase" behavior of a monolayer composed of ethanol molecules adsorbed at the vapor/ethanol-aqueous-solution interface was thoroughly investigated.[33] In this article, we report on additional analysis carried out on the structure of the solution at the interface, paying special attention to the cluster of molecules bound by HB. All analysis has been performed based on the adsorption-equilibrated configurations of the ethanol solution slab at 298.15 K, which is a continuation of our previous work.[33] The relatively large size of the bulk solution enabled a direct comparison of the structural properties at the interface with that of the bulk solution. The structure of this article is as follows. In Section 2, the methodology of the MD calculation is briefly reviewed. The main part of this article is in Section 3, where the result of the analysis of an ethanol one-component cluster and an ethanol/water binary cluster at the interface are formulated, comparing these clusters with those in the bulk solution. In Section 4, we will make some final remarks.

2. Simulation Method

The details of the MD calculation are the same as discussed in our previous work.[33] The intermolecular and intramolecular interactions were approximated by the optimized potential for liquid simulation (OPLS) potential model in the united atom form[34] for ethanol, and the rigid body single-point charge-extended (SPC/E) potential model[35] for water. Using this potential combination, we constructed an initial configuration where a 100 Å thick slab of ethanol solution by 10 Å pure water surface were placed at the center of a periodic unit cell that has a dimension of 40 Å × 40 Å × 240 Å.

To clarify the molar dependence of the MD results, five independent initial configurations were constructed in which the initial ethanol molar fraction of the 100 Å thick bulk solution layer was set to 0.010, 0.022, 0.045, 0.100, and 0.200, respectively. These initial configurations were composed of 18 465, 18 735, 17 977, 16 929, and 14 938 atoms, respectively.

In the MD calculation, the Lennard-Jones interaction was cut off at 13.3 Å. The Coulombic interaction was fully calculated by the Ewald summation technique.[36] Newton's equation of motion was numerically solved by the leapfrog algorithm with $\Delta t = 2$ fs. The interatomic lengths and angles were kept constant via the SHAKE algorithm.[37] The temperature of the system was controlled with the Berendsen thermostat.[38]

All MD calculations were performed with a homemade program optimized for the use of the MDGRAPE-2 board.[39] As in our previous work,[33] it was confirmed that by 15 ns *NVT* constant MD calculation (*N*: number of atoms, *V*: volume of calculation unit cell, *T*: temperature, $T = 298.15$ K), every system reached an equilibrium state of adsorption in which the ethanol mole fraction of the bulk solution χ_e became 0.0052, 0.012, 0.024, 0.057, and 0.12, respectively. After the establishment of an adsorption equilibration, an additional data-gathering 3 ns *NVT* constant MD run was performed for each χ_e case, saving the information about the coordinates and velocities of all atoms to a file every 0.1 ps. All analysis reported in this article was conducted based on these stock configuration files.

The notations about the geometry of the unit cell follows what was used in our previous work; e.g., the *z* axis was taken to be the direction perpendicular to the interface.

TABLE 1: Structual Properties of the Vapor/Ethanol-Aqueous-Solution Interface

χ_e^{33}	σ_e, Å^{33}	$\lvert z_e^0 - z_G \rvert$, Å
0.0052	3.7 (±0.1)	0.05[a]
0.012	4.1 (±0.1)	0.14[b]
0.024	4.6 (±0.1)	1.05[b]
0.057	5.6 (±0.1)	1.40[b]
0.12	6.5 (±0.4)	1.22[b]

[a] z_G is located on the vapor side of z_e^0. [b] z_G is located on the bulk solution side of z_e^0.

3. Results and Discussion

3.1. Number Density Profiles. Profiles of the number density of ethanol and the water at an equilibrium state of adsorption have been discussed in detail elsewhere.[33] Table 1 shows a summary of the structual properties of the interface, where σ_e is the characteristic width of the distribution of adsorbed ethanol. It is confirmed that the relative differences between the position of the peak of adsorbed ethanol distribution, z_e^0, and the position of the Gibbs dividing surface (GDS), z_G, depends on χ_e, the values of which are also listed in Table 1. A schematic relationship of each of the number density profiles is shown in Figure 1 when $\chi_e = 0.024$. Here, the criteria of the *z* axis is reset to the position of the distribution peak of adsorbed ethanol.

It is convenient in the following discussion to define the area to which ethanol molecules belong. As in our previous work,[33] we originally defined the adsorption area, V_{ads}, bulk solution area, V_{bulk}, and vapor region, V_{vap}, based on σ_e and z_e^0:

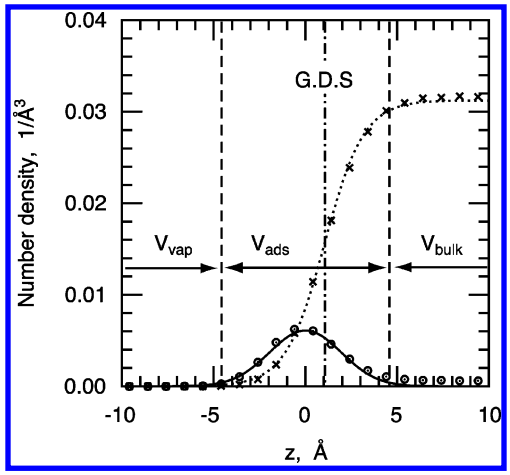

Figure 1. Profiles of number density at the vapor/liquid interface when $\chi_e = 0.024$: ethanol (open circles) and water (crosses). $z = 0$ corresponds to the position of the distribution peak of adsorbed ethanol. The dashed lines show the boundaries between V_{vap} and V_{ads}, and V_{ads} and V_{bulk}, respectively. The dotted−dashed line shows the position of the Gibbs dividing surface (GDS).

$$V_{ads} = \{z|z_e^0 - \sigma_e \le z \le z_e^0 + \sigma_e, z_e^{0\prime} - \sigma_e \le z \le z_e^{0\prime} + \sigma_e\} \quad (1)$$

$$V_{bulk} = \{z|z_e^0 + \sigma_e < z < z_e^{0\prime} - \sigma_e\} \quad (2)$$

$$V_{vap} = \{z|0 \le z < z_e^0 - \sigma_e, z_e^{0\prime} + \sigma_e < z \le L_z\} \quad (3)$$

where the prime shows the case of the another vapor/liquid interface (note that there are two vapor/solution interfaces in our calculation unit cell as shown in Figure 1 of ref 33). It has been confirmed that this original definition of V_{ads} provides a slight overestimation of the amount of soluble surfactant adsorbed in excess if compared with the case of the estimation through the Gibbs construction.[33]

3.2. Intermolecular Potential Energy. It is fundamentally desirable to estimate an intermolecular potential energy along the direction perpendicular to the interface. Figure 2 shows examples of profiles of the intermolecular potential energy of ethanol $U_e(z)$ and water $U_w(z)$, where the position of the mass center of each kind of molecule is adopted as a point in the process of the profile estimation. Profiles of the potential energy using a pair of molecular species $U_{ee}(z)$ (ethanol−ethanol), $U_{ew}(z)$ (ethanol−water), and $U_{ww}(z)$ (water−water) are also shown. A relative displacement from the position of the peak of adsorbed ethanol distribution was reset as the z axis. This resetting the z axis makes it convenient to discuss the results of our analysis when comparing it with the number density profiles.

In Figure 2, it is observed that $U_e(z)$ decreases monotonically at the vapor/solution interface toward V_{vap}, expressing two shoulders. The lower shoulder is located at the boundary between V_{vap} and V_{ads}, and its height is about −25 kJ/mol. This value is two times larger than the typical HB energy, regardless of χ_e. These tendencies are consistent with the MD results by Matsumoto et al.,[30] where they treated the vapor/methanol solution interface. The behavior of the higher shoulder is somewhat complicated, as it is located at the inside of V_{ads} when $\chi_e = 0.12$, but moves into the interior of V_{bulk} as χ_e decreases. Comparison with Figure 1 reveals that the position of the lower shoulder corresponds to the position at which the number density of water reaches its bulk value. This fact states that the potential energy of the ethanol molecules in solution is sensitive to the number density of water. $U_w(z)$ also has shoulders, and the

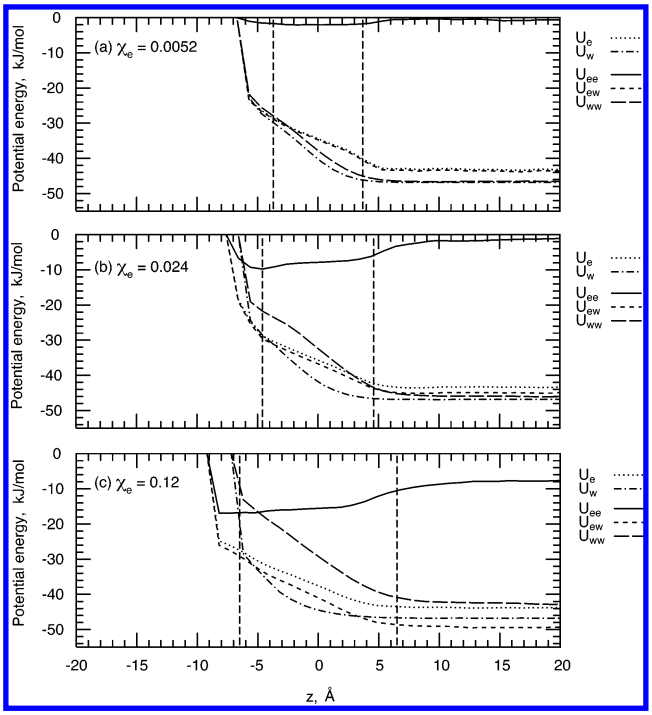

Figure 2. Profiles of intermolecular potential energies. The difference in line styles indicate differences in taking the pair of molecular species. χ_e is pictured in each figure. $z = 0$ corresponds to the position of the distribution peak of adsorbed ethanol. The dashed lines are the same in Figure 1.

height of the lower shoulder is about −25 kJ/mol. It is seen that the difference in χ_e affects the shape of $U_w(z)$ in V_{ads}. That is, the higher χ_e, the steeper $U_w(z)$ becomes in V_{ads}. This steepening may reflect the penetration of the region of bulk solution toward the interface. In contrast, $U_{ee}(z)$ presents a variation opposite to $U_e(z)$ and $U_w(z)$ in V_{ads}. It shows a gradual increase toward V_{vap}, with a maximum at the boundary between V_{ads} and V_{vap}. This fact indicates that the interaction between ethanol molecules is stabilized at the interface. The variation of $U_{ww}(z)$ in V_{ads} is similar to $U_w(z)$, while its absolute value monotonically decreases with χ_e. The variation of $U_{ew}(z)$ in V_{ads} is also similar to $U_e(z)$ and $U_w(z)$ but showing a peculiar variation with χ_e; i.e., its absolute value gradually increases with χ_e. In Section 3.3.2, discussion on the molecular origin of these results is presented, relating this to the coordination number of hydrogen bond.

The bulk value of the intermolecular potential energies can also be discussed. Table 2 shows the average values of $U_e(z)$, $U_w(z)$, $U_{ee}(z)$, $U_{ew}(z)$, and $U_{ww}(z)$ in V_{bulk}, denoted by $\langle U_e\rangle$, $\langle U_w\rangle$, $\langle U_{ee}\rangle$, $\langle U_{ew}\rangle$, and $\langle U_{ww}\rangle$, respectively. The values of $\langle U_w\rangle$ are constant despite χ_e and show close agreement with bulk value (−46.87 ± 0.05 kJ/mol[40]). This indicates that the amount of ethanol molecules does not have a strong influence on the overall energetics of water in V_{bulk} in the range of χ_e mentioned here. In contrast, the values of $\langle U_e\rangle$ gradually decreases with χ_e. This may be caused by structural variations both of the clustering form of ethanol molecules and of the solvation shell of water molecules around an ethanol molecule.

Details of the structural variation of solution with χ_e can be discussed with $\langle U_{ee}\rangle$, $\langle U_{ew}\rangle$, and $\langle U_w\rangle$. $\langle U_{ee}\rangle$ shows a rapid increase with χ_e, indicating that ethanol molecules tend to form clusters when χ_e is increased. In contrast, $\langle U_{ww}\rangle$ shows a gradual decrease with χ_e, indicating that the network of hydrogen-bonded water is continuously broken by addition of ethanol molecules. $\langle U_{ew}\rangle$ shows a gradual increase with χ_e,

TABLE 2: Averaged Values of Intermolecular Potential Energies in V_{bulk}

χ_e	$\langle U_e \rangle$, kJ/mol	$\langle U_w \rangle$, kJ/mol	$\langle U_{ee} \rangle$, kJ/mol	$\langle U_{ew} \rangle$, kJ/mol	$\langle U_{ww} \rangle$, kJ/mol
0.0052	−43.22 (±0.18)	−46.86 (±0.03)	−0.36 (± 0.23)	−43.64 (± 0.18)	−46.63 (± 0.08)
0.012	−43.23 (±0.14)	−46.86 (±0.01)	−0.69 (± 0.17)	−44.07 (± 0.14)	−46.45 (± 0.03)
0.024	−43.42 (±0.13)	−46.87 (±0.03)	−1.78 (± 0.63)	−45.02 (± 0.13)	−45.90 (± 0.29)
0.057	−43.61 (±0.08)	−46.85 (±0.03)	−4.27 (± 0.44)	−46.86 (± 0.08)	−44.63 (± 0.20)
0.12	−43.60 (±0.14)	−46.68 (±0.09)	−8.52 (± 0.61)	−49.04 (± 0.25)	−42.27 (± 0.36)

indicating that ethanol molecules are more stabilized by surrounding water molecules with χ_e. Some MD studies present a discussion on the function of solute molecules (methanol,[14] ethylene glycol, ethylenediamine, and 2-aminoethanol[41]) as a structure maker of water in a dilute solution with the object of $\langle U_{ww} \rangle$. Our MD results show that $\langle U_{ww} \rangle = -46.63$ kJ/mol when $\chi_e = 0.0052$, the absolute value of which is smaller than the bulk value (−46.87 kJ/mol). Thus, we state that ethanol does not have a function in the creation of the structure of water, at least over the noticed χ_e range. At the interface, we state the same conclusion.

The details of the clustering of ethanol molecule and the solvation structure of water due to HB are revealed in the next section.

3.3. Hydrogen Bond. Ethanol and water molecules can form HBs with its nearest neighboring ethanol and water molecules. In a MD study, the HBs are usually defined by calculating the intermolecular potential energy or relative geometry between two molecules. It has been confirmed that these two methodologies give almost the same pairs of hydrogen-bonded molecules, and therefore reports very similar dynamics of HB.[42,43]

In this study, we adopted the latter methodology to detect a pair of the molecules bound by HB based on the geometric criteria: A pair of ethanol molecules form a HB if the O−O distance is less than 3.5 Å, O−H distance is less than 2.6 Å, and the O−H···O angle is greater than 140°.[31,32] The set of criteria for an ethanol−water HB is 3.6 Å, 2.5 Å, and 140°, and 3.6 Å, 2.5 Å, and 140° for a water−water HB.[31,32] The criteria on the O−O and O−H distances are based on the position of the first minima of interatomic radial distribution functions, $g_{OO}(r)$ and $g_{OH}(r)$.[19,44,45] The criterion on the O−H···O angle reflects a linear arrangement of atoms in the pair of hydrogen-bonded molecules. In ref 31, it is reported that ethanol molecules form "loose" HB at the vapor/solution interface. In this paper, however, the "tight" definition of the HB based on the geometric criteria mentioned above are applied to the all molecule pairs regardless of their positions.

3.3.1. Density of Hydrogen Bond. Figure 3 shows profiles of the number of HBs per unit volume, i.e., the density of HB, $\rho_{HB}^{ee}(z)$, $\rho_{HB}^{ew}(z)$, and $\rho_{HB}^{ww}(z)$, respectively, where superscripts ee, ew, and ww show the cases of HB between ethanol−ethanol, ethanol−water, and water−water, respectively. The position of the mass center of a pair of hydrogen-bonded molecules is adopted as a point in the process of the profile estimation.

It is commonly observed that $\rho_{HB}^{ee}(z)$ and $\rho_{HB}^{ew}(z)$ have sharp peaks near the vapor/solution interface and that the peak of $\rho_{HB}^{ee}(z)$ always positions itself at the vapor side rather than that of $\rho_{HB}^{ew}(z)$. This indicates that an ethanol molecule has a strong tendency to swap molecules that it chooses to partake in HB with, depending on its z position. This selectivity of the HB partner can be linked with the characteristic orientation of an ethanol molecule at the vapor/solution interface. Experimental studies[23,25,26] and MD studies[31−33] have revealed that an ethanol molecule adsorbs to the vapor/solution interface with its hydrophobic methyl tail sticking out toward the vapor side and its hydrophilic hydroxyl head penetrating the solution. Naturally, it is possible to conclude that, as the ethanol molecules penetrate deeper into the solution phase, the number of hydroxyl groups that contact a water molecule gradually increases. The difference in the position of the peaks of $\rho_{HB}^{ee}(z)$ and $\rho_{HB}^{ew}(z)$ should be attributable to the distinguishable environments of water molecules around the ethanol molecules at z.

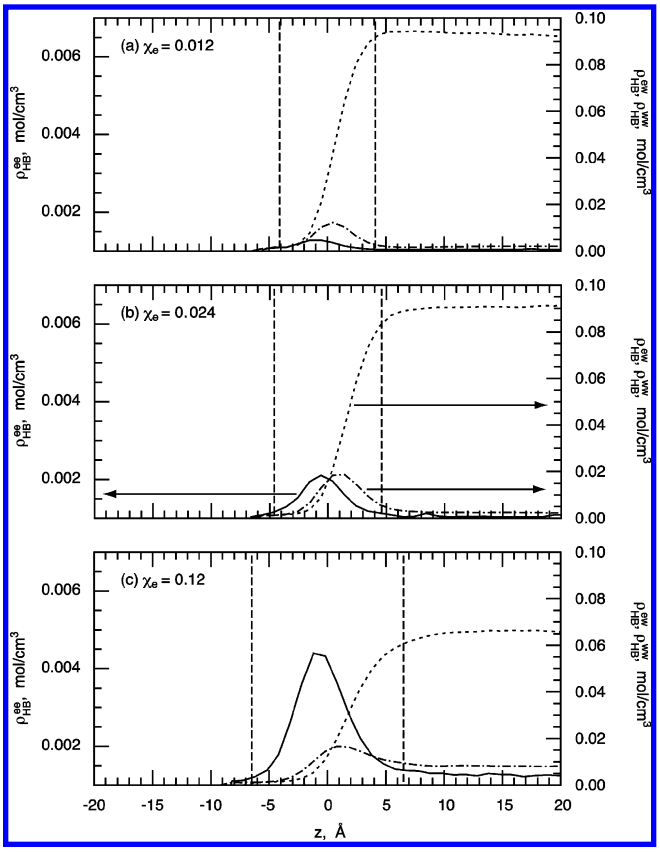

Figure 3. Profile of the density of hydrogen bond: ethanol−ethanol (solid line), ethanol−water (dotted−dashed line), and water−water (dotted line). χ_e is pictured in each figure. $z = 0$ corresponds to the position of the distribution peak of adsorbed ethanol. The dashed lines are the same as in Figure 1.

Consequently, we suggest the picture of an adsorbed monolayer to be composed of two subareas. In the one subarea, located at the vapor side of z_0, ethanol molecules prefer to form HBs with each other, while in the other subarea, located on the solution side of z_0, ethanol molecules prefer to make HBs with water molecules. It should be noticed here that the number density of ethanol itself is almost the same in both subareas (see also Figure 1). The former subarea is denoted by V_{ads}^{v}, and the latter subarea is denoted by V_{ads}^{b} in the following discussion.

On the other hand, the bulk value of the density of HB, $\langle \rho_{HB} \rangle$, may be obtained as the average of $\rho_{HB}(z)$ over V_{ads}. Figure 4 shows the variation of $\langle \rho_{HB}^{ee} \rangle$, $\langle \rho_{HB}^{ew} \rangle$, and $\langle \rho_{HB}^{ww} \rangle$ with χ_e. It is seen that $\langle \rho_{HB}^{ee} \rangle$, and $\langle \rho_{HB}^{ew} \rangle$ become monotonically increasing functions of χ_e, while $\langle \rho_{HB}^{ww} \rangle$ becomes a monotonically decreasing function of χ_e. The nonzero convergence of $\langle \rho_{HB}^{ee} \rangle$ in a dilute limit is also observed, which implies that there is a small number of ethanol clusters in a very dilute region of

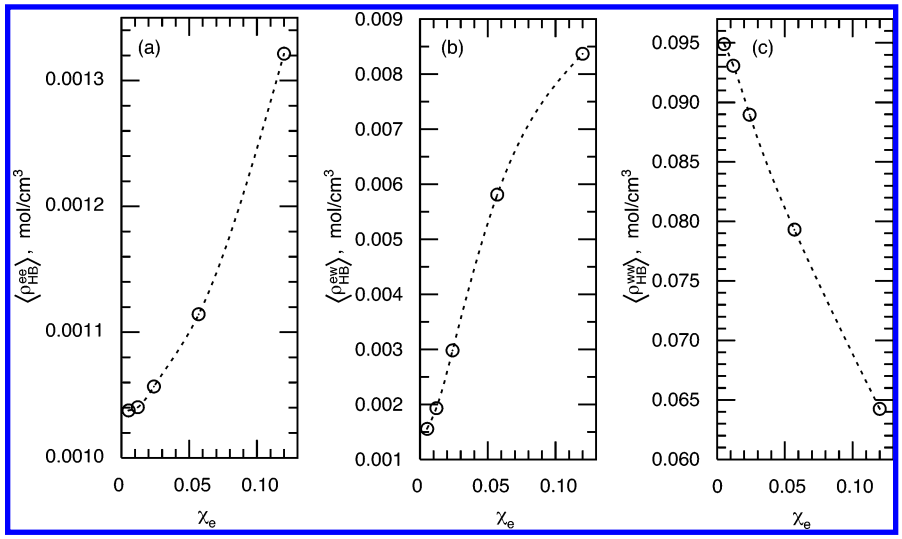

Figure 4. Bulk value of the density of hydrogen bond as a function of χ_e: (a) $\langle \rho_{HB}^{ee} \rangle$, (b) $\langle \rho_{HB}^{ew} \rangle$, and (c) $\langle \rho_{HB}^{ww} \rangle$. The dotted lines are curves fit using cubic spline interpolation.

ethanol. This result is consistent with previous MD studies on methanol,[16] 1-propanol,[20] and *tert*-butyl alcohol[22] solutions, where the clustering of alcohol molecules over a very dilute region was observed. It is also expected that $\langle \rho_{HB}^{ew} \rangle$ will converge to a nonzero value in the dilute limit. This is not improbable because the hydrophilic hydroxyl part of ethanol has the tendency to form HBs with water molecules. In contrast, $\langle \rho_{HB}^{ww} \rangle$ decreases almost linearly with χ_e. This will reflect the breaking of the hydrogen-bonded network of water molecules by the addition of ethanol molecules.

3.3.2. Coordination Number of Hydrogen Bond. It is interesting to reveal the coordination number of HB, n_{HB}, which was estimated simply by counting the number of molecular pairs taking place in HB. Figure 5 shows examples of the profile of the coordination number of HB, $n_{HB}^{ee}(z)$, $n_{HB}^{ew}(z)$, and $n_{HB}^{ww}(z)$, where the superscripts have the same meaning as that found in the previous section. The position of the mass center of the ethanol molecule is adopted as a point in the process of the profile estimation.

It is commonly observed that $n_{HB}^{ee}(z)$ gradually rises in V_{ads} toward V_{vap}, while $n_{HB}^{ew}(z)$ and $n_{HB}^{ww}(z)$ gradually decrease in the same region. It is speculated that the variation of n_{HB}^{ee} reflects the change of the composition of ethanol one-component clusters in V_{ads}. The continuous changes of $n_{HB}^{ew}(z)$ also indicate that the composition of ethanol/water binary clusters in V_{ads} also depend on the position of ethanol molecule. The details of the cluster composition of ethanol one-component clusters and ethanol/water binary cluster will be discussed in Section 3.3.3. It may be noted that there are unusual features in the shapes of n_{HB}^{ee}, n_{HB}^{ew}, and n_{HB}^{ww}, i.e., they have steep cliffs near the boundary between V_{vap} and V_{ads}. This is due to the paucity of molecule in V_{vap}. Therefore, if a longer MD calculation was carried out, it is expected that these profiles would become smoother.

The bulk values of n_{HB} are also discussed. Figure 6 shows the molar dependency of the coordination number of HB averaged over V_{bulk}, which are denoted by $\langle n_{HB}^{ee} \rangle$, $\langle n_{HB}^{ew} \rangle$, and $\langle n_{HB}^{ww} \rangle$. It is apparent that $\langle n_{HB}^{ee} \rangle$ becomes a monotonically increasing function of χ_e, while $\langle n_{HB}^{ew} \rangle$ and $\langle n_{HB}^{ww} \rangle$ become monotonically decreasing function of χ_e. The behaviors of $\langle n_{HB}^{ee} \rangle$ and $\langle n_{HB}^{ew} \rangle$ correspond to those of the Kirkwood−Buff parameters defined by[46]

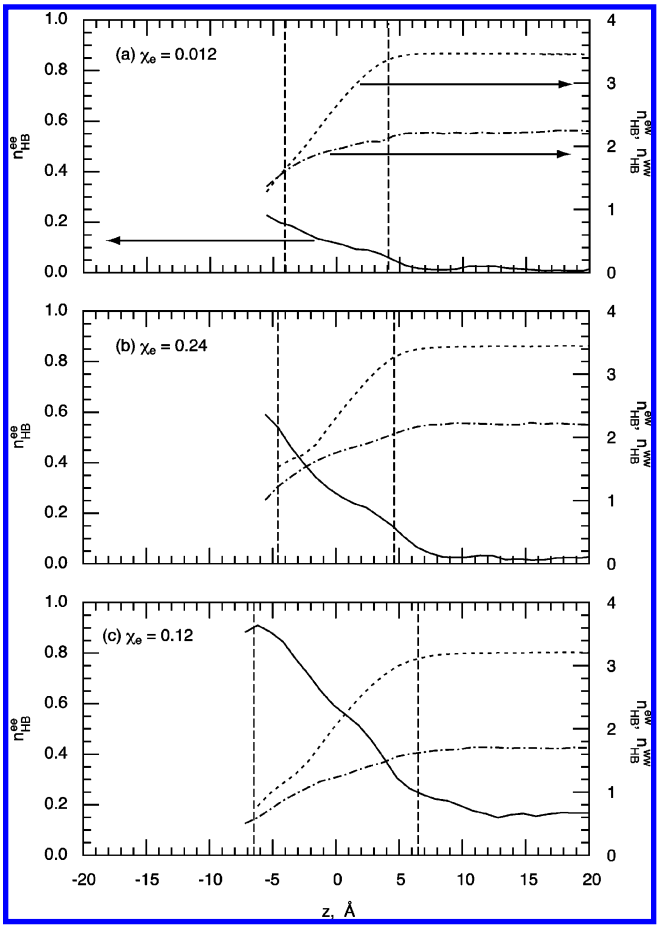

Figure 5. Profiles of the coordination number of hydrogen bond: ethanol-ethanol (solid line), water−water (dotted line), and ethanol−water (dashed doble dotted line). χ_e is pictured in each figure. $z = 0$ corresponds to the position of the distribution peak of adsorbed ethanol. The dashed lines are the same as in Figure 1.

$$G_{\alpha\beta} = \int_0^\infty (g_{\alpha\beta}(r) - 1)\, 4\pi r^2\, dr \qquad (4)$$

where $g_{\alpha\beta}(r)$ is the radial distribution function between α and β molecular species. The ethanol−ethanol Kirkwood−Buff parameter G_{ee} shows rapid increase with χ_e, while that of ethanol−water G_{ew} shows gradual decrease in the range of $\chi_e < 0.15$.[1−4] Contrastingly, the behavior of $\langle n_{HB}^{ww} \rangle$ is opposite to

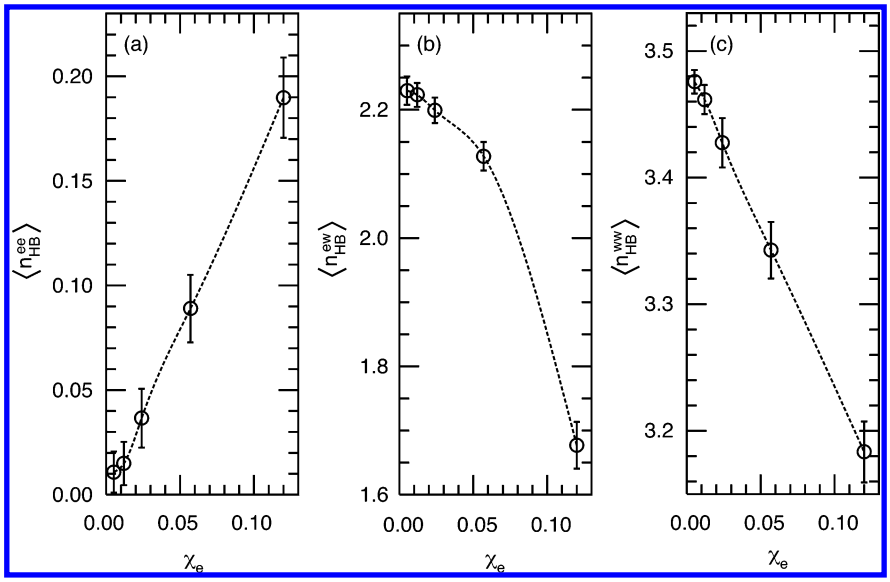

Figure 6. Bulk value of the coordination number of hydrogen bond as a function of χ_e: (a) $\langle n_{HB}^{ee} \rangle$, (b) $\langle n_{HB}^{ew} \rangle$, and (c) $\langle n_{HB}^{ww} \rangle$. The dotted lines are curves fit using cubic spline interpolation.

G_{ww}, which implies that a long-ranged water−water correlation dominates the behavior of G_{ww}.

In Figure 6, a nonzero convergence of $\langle n_{HB}^{ee} \rangle$ in the dilute region is expected, which is complementary to $\langle \rho_{HB}^{ee} \rangle$ (see also Figure 4). This is further evidence that there are a few ethanol clusters even in the dilute limit. The linear increase of $\langle n_{HB}^{ee} \rangle$ and linear decrease of $\langle n_{HB}^{ww} \rangle$ indicates that the addition of ethanol enhances the self-clustering of ethanol and breaking of the hydrogen-bonded network of water in the solution. A distinguishing note is that $\langle n_{HB}^{ew} \rangle$ is a quadratic function of χ_e, being convex upward. It is considered that a rapid decrease of $\langle n_{HB}^{ew} \rangle$ in higher χ_e regions will be caused by a growth in the aggregation of ethanol molecules via the hydroxyl groups and the consequent decrease of the contant frequency of water molecules with the hydroxyl group.

$n_{HB}^{ee}(z)$, $n_{HB}^{ew}(z)$, and $n_{HB}^{ww}(z)$ partially explain the molecular origin of variation of $U_{ee}(z)$, $U_{ew}(z)$, and $U_{ww}(z)$ in V_{ads} and their χ_e dependence. In general, the increase of the coordination number of HB results in the stabilization of a pair of molecular species. Thus, it can be assumed that the gradual rise of $n_{HB}^{ee}(z)$ in V_{ads} toward V_{vap} results in a gradual decrease of $U_{ee}(z)$ in V_{ads}. The variation of $U_{ww}(z)$ in V_{ads} and χ_e dependence of $\langle U_{ee} \rangle$ and $\langle U_{ww} \rangle$ are explained by the same mechanism. On the other hand, the decrease of $U_{ew}(z)$ with χ_e is not explained by $n_{HB}^{ew}(z)$: $U_{ew}(z)$ decreases with χ_e, although $n_{HB}^{ew}(z)$ also decreases. This inconsistency may be caused by the situation where ethanol molecules are stabilized not only by the direct HB with water molecules but also by an indirect contribution from surrounding water molecules.

3.4. Composition of the Hydrogen-Bonded Cluster. As is implied in Section 3.3.2, the composition of the cluster of molecules dominates the hydrogen-bonded structure of the ethanol-aqueous-solution. In this section, the compositions of an ethanol one-component cluster and ethanol/water binary cluster are thoroughly investigated at the interface and in the bulk solution.

It is easy to detect the clusters of molecules linked to each other by HB if the list of a pair of the molecules bound by HB were obtained. For example, the usage of the list of the molecule pair of ethanol−ethanol or water−water HB may enable the detection of one-component clusters of ethanol or water, respectively. It is also possible to detect binary clusters, such as an ethanol-cored ethanol/water binary cluster and a patched binary cluster in which intervenient water molecules bridge a gap between linear ethanol clusters, using the combination of an ethanol−ethanol HB molecule pair list and an ethanol−water HB molecule pair list. However, we have limited the following discussion to only two kinds of clusters. One is the ethanol one-component cluster, and the other is the ethanol/water binary cluster noted above. This is why the water molecules in the slab of solution steadily percolates as far as we use the geometric definition of HB described above. It should be mentioned that only the water molecules that belong to the first neighboring shell around the hydroxyl part of the ethanol molecule are included in the ethanol/water binary cluster detected here. The binary cluster defined here is similar to that by Roney et al.[20]

3.4.1. Ethanol One-Component Cluster. Figure 7 shows examples of the profiles of the mean size of an ethanol one-component cluster, $s_{mean}^{e}(z)$. The profiles of the number density of the ethanol one-component cluster, $\rho_{cls}^{e}(z)$, are also shown in Figure 7. The position of the mass center of the ethanol one-component cluster is adopted as a point in the process of the profile estimation.

The common features in $s_{mean}^{e}(z)$ include the appearance at the boundary between V_{bulk} and V_{ads}, having a maximum in V_{ads}^{v}, and finally converging to unity in V_{vap}. It is interesting that the similar tendency has been observed in $\rho_{cls}^{e}(z)$, but the positions of their maximums do not correspond with each other; i.e., The maximum of $s_{mean}^{e}(z)$ is located in V_{ads}^{v}, while the position of the peak of $\rho_{cls}^{e}(z)$ only corresponds to $z = 0$. These results introduce a molecular picture where there are the largest number of ethanol clusters near $z = 0$ with their sizes being relatively small, while there are the large-sized but relatively small number of ethanol clusters in V_{ads}^{v}.

The detailed contents of the variation of $s_{mean}^{e}(z)$ in V_{ads} can be examined by the profile of the size distributions of the ethanol cluster, $p_s^e(z)$, which are shown in Figure 8. The ratio of monomer to all of the clusters, p_1^e, started to decrease at the boundary of V_{bulk} and V_{ads} with its minimum in V_{ads}^{v}, while the ratio of each oligomer, p_s^e ($s \geq 2$), expressed its maximum at the same position. It is apparent that the increase of χ_e, which

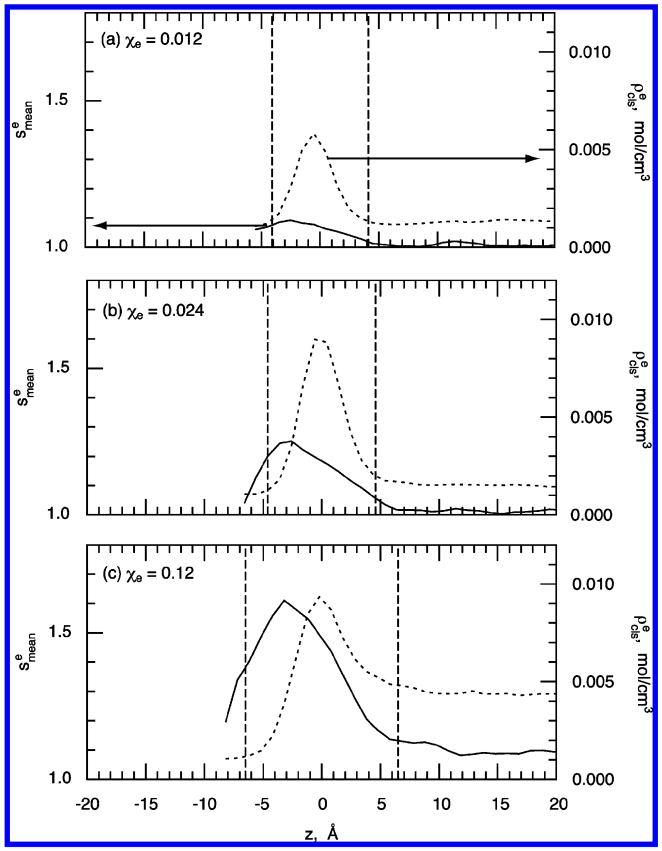

Figure 7. Profiles of the mean size of an ethanol one-component cluster, s^e_{mean}, and its number density, ρ^e_{cls}. χ_e is pictured in each figure. $z = 0$ corresponds to the position of the distribution peak of adsorbed ethanol. The dashed lines are the same as in Figure 1.

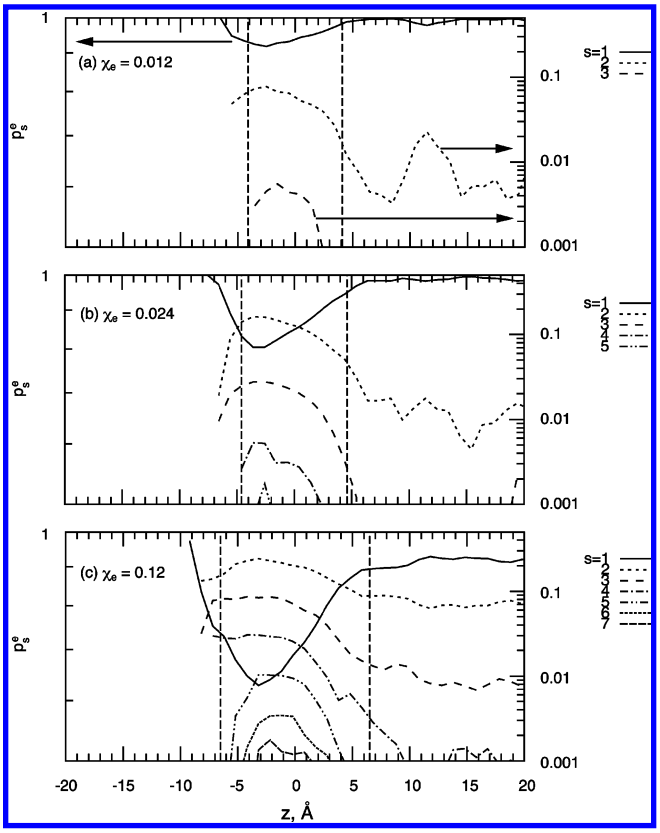

Figure 8. Profiles of the distribution of an ethanol one-component cluster. The difference in line styles indicate differences in sizes, s. χ_e is pictured in each figure. $z = 0$ corresponds to the position of the distribution peak of adsorbed ethanol. The dashed lines are the same as in Figure 1.

should result in the increase in adsorption amounts induces an abundance in the kind of oligomers present, with their ratios increasing. For instance, about 90% of the ethanol exists as monomers at positions of extremum, and the remaining 10% of the ethanol exist as dimers when $\chi_{eth} = 0.012$. In contrast, only about 60% of the ethanol exist as monomers, and the remaining 25, 9, and 3% of the ethanol exists as dimers, trimers, and tetramers, respectively, when $\chi_{eth} = 0.12$.

Taking this into consideration, it can be stated that the maximization of $s^e_{mean}(z)$ in V_{ads} is caused by the disappearance of the monomer and the consequent formation of oligomers, especially *dimers*. It can also be stated that the monotonic increase of n^{ee}_{HB} in V_{ads} toward V_{vap} is caused by the same process. That is, the ratio of each oligomer in which some intermolecular HBs are present shows its maximum at the boundary between V_{ads} and V_{vap}, resulting in the maximization of n^{ee}_{HB}. The increase in n^{ee}_{HB} with χ_e is caused by the diversity of the kind of oligomers present and in the increase in their ratios with χ_e.

The bulk properties of $s^e_{mean}(z)$ and $p^e_s(z)$ can also be discussed. These average values over V_{bulk}, $\langle s^e_{mean}\rangle$ and $\langle p^e_s\rangle$, are shown in Figure 9. It is apparent that $\langle s^e_{mean}\rangle$ monotonically increases with χ_e, the qualitative behavior of which is very similar to $\langle n^{ee}_{HB}\rangle$. This similarity is plausible because an increase in the coordination number of ethanol−ethanol HB is expected to result in the increase of the size of ethanol one-component clusters. The nonunity convergence of $\langle s^e_{mean}\rangle$ in the dilute limit is also apparent. This is conclusive evidence that there are few ethanol oligomers in the dilute limit. The relatively large error bars indicate that the size of ethanol clusters fluctuates widely in the bulk solution. Detailed discussions can

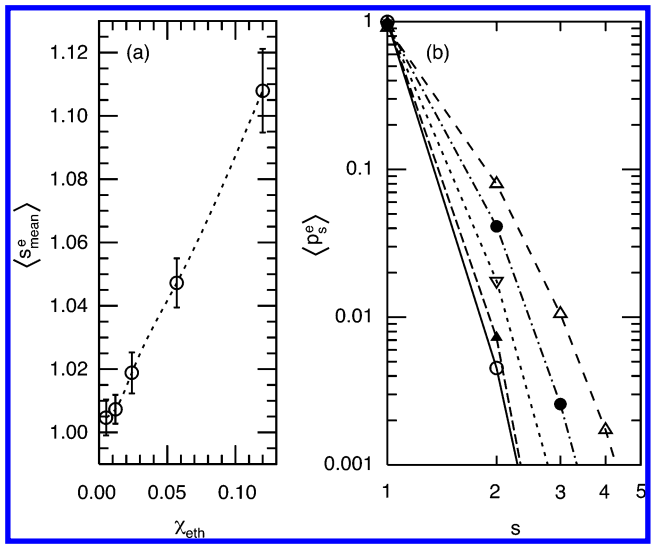

Figure 9. Bulk properties of an ethanol one-component cluster: (a) the mean size as a function of χ_e, and (b) the size distribution in each χ_e. In (a), the dotted line is a curve fit using cubic spline interpolation. In (b), the open circles, closed triangles, inversed open triangles, closed circles, and open circles correspond to the cases where $\chi_e = 0.0052$, 0.012, 0.024, 0.057, and 0.12, respectively.

be made with $\langle p^e_s\rangle$. In the solution of $\chi_e = 0.0052$ and 0.012, 99% of the ethanol exists as a monomer. The percentage of ethanol monomer present gradually decreases with χ_e, but 90% resides as a monomer even when $\chi_e = 0.12$. The most populated oligomer is a dimer, the percentage of which varies on the order of 1%. The percentages of the other oligomers are less than 1% even in the most concentrated χ_e. These observa-

tions lead to the conclusion that the variation of $\langle s^{e}_{mean} \rangle$ is mainly contributed by the formation of the ethanol dimer and not because of the other oligomers, as in the case at the interface. The resuts of $\langle s^{e}_{mean} \rangle$ and $\langle p^{e}_{s} \rangle$ agree well with experimental studies by Nishi et al.[7,8] They hypothesized that a tiny amount of ethanol dimer is formed even in very dilute solutions ($\chi_e = 0.001$) and the size of ethanol clusters is lengthened with χ_e. As $\langle p^{e}_{s} \rangle$ indicates, less than 1% of ethanol exists as a dimer in a dilute limit.

It is instructive to compare the above results with the MD study on supercritical fluids.[47,48] This is because an ambient condition for miscible alcohol solutions is assumed to remain above the critical temperature below which the two liquids are not miscible in all proportions.[49] Mountain investigated void sizes in supercritical water, showing that there are voids with a size of an integer multiple of methane diameters (~3.43 Å).[47] The void size distribution p^{v}_{s} was also estimated, which becomes a monotonically decreasing function of the void size s^{v}. Dellis et al. investigated pressure and temperature dependence of the hydrogen bonding in supercritical ethanol.[48] They found that supercritical ethanol is basically formed by a significant number of monomer molecules, while the rest of them are hydrogen bonded primarily in dimers and trimers as well as a markedly small number of tetramers. $\langle p^{e}_{s} \rangle$ shown in Figure 9 corresponds qualitatively to these results if we make a simple assumption that a miscible ethanol solution is composed of supercritical water with the voids filled with supercritical ethanol.

3.4.2. Ethanol/Water Binary Cluster. Figure 10 shows examples of profiles of the mean size of the ethanol/water binary cluster, $s^{ew}_{mean}(z)$ and their number density, $\rho^{ew}_{cls}(z)$. For more detailed information, the mean sizes of the ethanol component of the binary cluster and the water component of the binary cluster are profiled along the z axis. The position of the mass center of the binary cluster is adopted as a point in the process of the profile estimation. It should be noticed that the minimum size of the binary cluster is 2 by its own definition.

It is apparent that $s^{ew}_{mean}(z)$ increases at the boundary between V_{ads} and V_{bulk}, and then a maxima is expressed near $z = 0$. After that, convergence to zero occurs in a discontinuous manner at the boundary between V_{ads} and V_{vap}. These qualitative behaviors are similar to those of $s^{e}_{mean}(z)$, but there are some differences in their detailed shapes. In particular, the position of the peaks of both $s^{ew}_{mean}(z)$ and $\rho^{ew}_{cls}(z)$ located at the solution side of those of $s^{e}_{mean}(z)$ and $\rho^{e}_{cls}(z)$. We suggest that these differences come from the differences in the geometric shapes of each type of cluster. It is speculated that the ethanol/water binary cluster has a shape in which water molecules are docked at the hydroxyl part along the z axis, which will result in a small deviation of its own mass center from $z = 0$. On the other hand, the ethanol one-component cluster is assumed to have a shape where each molecule is connected laterally, which will result in the large deviation of its own mass center from $z = 0$ toward V_{ads}. The behaviors of the ethanol component and water component of $s^{ew}_{mean}(z)$ provide further infomation supporting the above speculation. The former expresses its maximum at V^{v}_{ads}, while the latter expresses its maximum at V^{b}_{ads}, which should result from the situation that binary clusters have an anisotropic form in V_{ads}. Therefore, we conclude that the ethanol/water binary cluster has an anisotropy in its shape along the z axis, which causes small deviations of the position of the maximum of $s^{ew}_{mean}(z)$ from $z = 0$, unlike in the case of s^{e}_{mean}. This anisotropy might

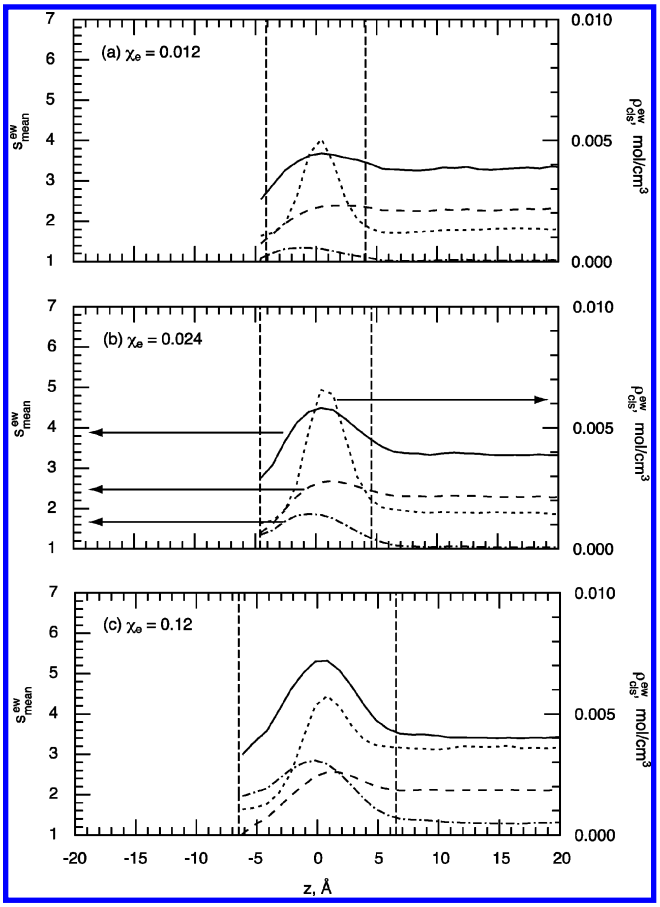

Figure 10. Profiles of the mean size of an ethanol/water binary cluster, s^{ew}_{mean}: whole part (solid lines), ethanol component (dotted−dashed lines), and water component (long-dashed lines). Number density profiles of the binary cluster, ρ^{ew}_{mean}, are also depicted in each figure (dotted lines). χ_e is pictured in each figure. $z = 0$ corresponds to the position of the distribution peak of adsorbed ethanol. The dashed lines are the same as in Figure 1.

be discovered by comparing the results of ρ^{ee}_{HB} and ρ^{ew}_{HB}, as discussed in the Section 3.3.1.

A more detailed discussion can be made, analyzing the size distribution of the binary clusters, p^{ew}_{s}. Figure 11 shows examples of the profiles of $p^{ew}_{s}(z)$. In contrast to $p^{e}_{s}(z)$, the ratio of binary dimer to the all binary clusters, p^{ew}_{2}, started to increase at the boundary between V_{ads} and V_{bulk}, while the ratios of binary trimers and tetramers, p^{ew}_{3} and p^{ew}_{4}, decreased and the ratios of binary oligomers whose sizes are greater than 5 increased. Another feature is that the profile of the dimer, trimer, and tetramer did not show any extrema in V_{ads}, while the other oligomers expressed their maxima at the same position of the maximum in $\rho^{ew}_{cls}(z)$. The increase of χ_e caused the diversity in the types of oligomers in V_{ads}, but the percentage of which did not grow remarkably. Taking this into consideration, we deduce that the maximum in $s^{ew}_{mean}(z)$ is a product of the competition of many kinds of oligomers, which is quite a contrast to the case of $s^{e}_{mean}(z)$, where the generation of the dimer played a dominating role. The variation of $n^{ew}_{HB}(z)$ in V_{ads} can be also exposed, relating this to the variations of $p^{ew}_{s}(z)$. The observed results include $p^{ew}_{2}(z)$ asymptotically approaching unity toward V_{vap}, and $p^{ew}_{3}(z)$ and $p^{ew}_{4}(z)$ monotonically decreasing. It is trivial to show that the ethanol molecule contained by the binary dimer has the smallest coordination number of ethanol−water HB, i.e., unity. Therefore, the gradual domination of the dimer toward V_{vap} must cause a decrease in n^{ew}_{HB}. The monotonic

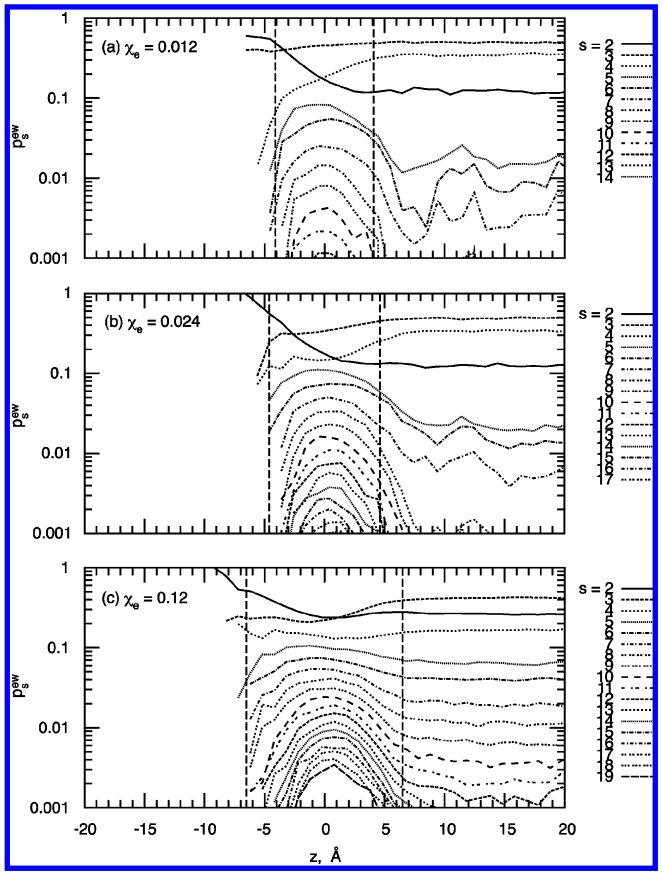

Figure 11. Profiles of the size distribution of an ethanol/water binary cluster. Differences in line styles indicate differences in their sizes, s. χ_e is pictured in each figure. $z = 0$ corresponds to the position of the distribution peak of adsorbed ethanol. The dashed lines are the same as in Figure 1.

decrease of n_{HB}^{ew} toward V_{vap} may be the product of the competition between the formation of various sizes of oligomers in V_{ads}.

In the last section of this article, details regarding the structure of the ethanol/water binary cluster in the bulk solution are discussed. Figure 12a shows the spatial average of $s_{mean}^{ew}(z)$ over V_{bulk}, $\langle s_{mean}^{ew}\rangle$, as a function of χ_e, where the fraction of the water component to ethanol component, $f_{w/e}$, is also shown. It is shown that $\langle s_{mean}^{ew}\rangle$ is *not* a monotonically increasing function of χ_e, and there are two characteristic mole fractions where $\langle s_{mean}^{ew}\rangle$ changes its behavior. In $\chi_e \le 0.012$, $\langle s_{mean}^{ew}\rangle$ was almost constant in value ($\sim$3.29), but then started to increase drastically. After that, it reached its maximum ($\sim$3.6) near $\chi_e = 0.05$, and then started to decrease with χ_e. This behavior of $\langle s_{mean}^{ew}\rangle$ is quite different from that of $\langle s_{mean}^{e}\rangle$, which was a monotonically increasing function of χ_e. It is also interesting that $f_{w/e}$ becomes a monotonically decreasing function of χ_e. This implies that the ethanol molecules higher in χ_e in solution prefer to aggregate toward each other, partially forming a core of ethanol surrounded by water molecules. The enhanced decrease of n_{HB}^{ew} in high χ_e regions shown in Figure 6 backs up this implication.

The reason $\langle s_{mean}^{ew}\rangle$ expresses this behavior can be shown by considering the size distribution of the binary cluster averaged over V_{ads}, $\langle p_s^{ew}\rangle$. Figure 12b shows $\langle p_s^{ew}\rangle$ as a function of s. Again, it is noted that the minimum in s is 2 by its definition. In $\chi_e \le 0.012$, $\langle p_s^{ew}\rangle$ have similar shapes, except over the range $s \ge 5$, which results in a minimal rise of $\langle s_{mean}^{ew}\rangle$. In the range of $0.012 < \chi_e < 0.05$, the decrease in $\langle p_4^{ew}\rangle$ and increase in $\langle p_s^{ew}\rangle$ of $s \ge 5$ are shown, which leads to the growth of

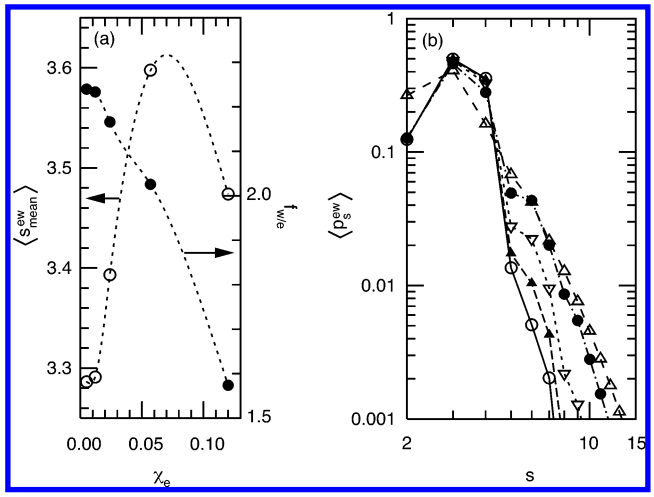

Figure 12. Bulk properties of an ethanol/water binary cluster: (a) The mean size as a function of χ_e, and (b) the size distribution in each χ_e. In (a), the fraction of water component to ethanol component, $f_{w/e}$ is also plotted. In (a), the dotted lines are curves fit using cubic spline interpolation. In (b), the open circles, closed triangles, inversed open triangles, closed circles, and open circles correspond to the cases where $\chi_e = 0.0052$, 0.012, 0.024, 0.057, and 0.12, respectively.

$\langle s_{mean}^{ew}\rangle$. At $\chi_e = 0.12$, $\langle p_s^{ew}\rangle$ of $s = 2$ and $s \ge 5$ raised relatively, while $\langle p_s^{ew}\rangle$ of $s = 3$, 4 declined, which led to the decrease in $\langle s_{mean}^{ew}\rangle$. The increase of $\langle s_{mean}^{ew}\rangle$ in the range of $\chi_e < 0.05$ contributes to the minimal variation of $\langle p_s^{ew}\rangle$ with χ_e, while the decrease of $\langle s_{mean}^{ew}\rangle$ in the range of $\chi_e > 0.05$ contributes to the major variation in $\langle p_s^{ew}\rangle$ with χ_e.

A comparison of $f_{w/e}$ with MS studies[7−9] is beneficial. Nishi et al.[8] suggest that $f_{w/e} = 2 \pm 1$ when $\chi_e = 0.02$. Our MD result of $f_{w/e}$ is 2.2, which agrees well with the experimental result. This close agreement is surprising because they insist that the main contribution to $f_{w/e}$ is given by the binary clusters having the core of ethanol hexamer, heptamer, and octamer, which are never detectable in our MD calculation (see Figure 12b).[8] They provided the molecular picture that the ethanol core of binary cluster is made of stacked ethyl groups, being closely located to each other due to the tension from the strong network of the outer water molecules coupled with the OH group of ethanols. These water molecules are assumed to form one (or two) layer(s) of a mantle-type HB network around an ethanol core and should be surrounded by bulk water. The close agreement in $f_{w/e}$ indicates that our definition of ethanol/water binary clusters corresponds roughly to that by Nishi et al., although our definition does not necessarily assume the formation of an ethanol core like the suggestion by Wakisaka and Ohki.[9] It should be considered that the spatial scale of phenomenon by their MS experiment (segmentation of ethanol/water binary clusters by an adiabatic expansion of solution droplet with a diameter of a few μm) is quite large if compared with the dimension of our MD calculation system. This will be the reason ethanol hexamer, heptamer, and octamer are detectable in the MS experiment; i.e., segmented binary cluster by an adiabatic expansion of a solution droplet will be composed of plurality of the binary cluster by our definition. To solve this issue, it is greatly expected to carry out a huge-scale MD calculation imitating the adiabatic expansion of a solution droplet.

4. Conclusions

We have carried out MD calculations where the structure of the vapor/ethanol-aqueous-solution interface was carefully investigated. The structure of the solution was clarified by

considering an intermolecular hydrogen bond and a molecular cluster bound by hydrogen bonds. To promote analysis in a unified manner, the position of the peak of adsorbed ethanol distribution, z_0, and the width of the distribution, σ_e, were adopted as the criteria used to measure the depth from the interface. Analysis on the density of HBs revealed that a monolayer of adsorbed ethanol can be classified into two parts at a molecular level. In the part positioned on the vapor side of z_0, ethanol molecules prefer to hydrogen bond to each other. In the other part positioned on the solution side of z_0, ethanol molecules prefer to form hydrogen bonds with water molecules. It is suggested that this selectivity of the HB partner along the depth from the interface results from the characteristic orientation of an ethanol molecule at the vapor/solution interface. The variation of the coordination number of HB and the mean size of molecular clusters at the interface are successfully explained via the size distribution of molecular cluster. At the interface, the decrease in ethanol monomers toward the vapor region and consequent increase of ethanol oligomers, especially ethanol dimers, occurs, which results in an increase in the coordination number of ethanol−ethanol HB toward the vapor region. A maximization in the size of an ethanol one-component cluster mainly contributes to the formation of dimers. On the other hand, the increase of the ethanol/water binary dimer toward the vapor region and the decrease of the binary trimer and tetramer occurs, which results in a decline in the coordination number of ethanol−water HB toward the vapor region. A maximization in the size of the ethanol/water binary cluster is the product of the competition between the formation of various sizes of the binary oligomer. The molar dependency of structural properties described above in the bulk solution was also discussed, the details of which are described in the body text.

Acknowledgment. This research is supported by the Core Research for Evolutional Science and Technology (CREST) of the Japan Science and Technology Corporation (JST). This work is supported in part by a grant in aid for the 21st Century Center of Excellence for "System Design: Paradigm Shift from Intelligence to Life" from the Ministry of Education, Culture, Sport, and Technology in Japan.

References and Notes

(1) Ben-Naim, A. *J. Chem. Phys.* **1977**, *67*, 4884.
(2) Donkersloot, M. C. A. *J. Solution Chem.* **1979**, *8*, 293.
(3) Matteoli, E.; Lepori L. *J. Chem. Phys.* **1984**, *80*, 2856.
(4) Nishikawa, K.; Iijima, T. *J. Phys. Chem.* **1993**, *97*, 10824.
(5) Onori, G. *J. Chem. Phys.* **1988**, *89*, 4325.
(6) D'Angelo, M.; Onori, G.; Santucci, A. *J. Chem. Phys.* **1994**, *100*, 3107.
(7) Nishi, N.; Koga, K.; Ohshima, C.; Yamamoto, K.; Nagashima, U.; Nagami, K. *J. Am. Chem. Soc.* **1988**, *110*, 5246.
(8) Nishi, N.; Takahashi, S.; Matsumoto, M.; Tanaka, A.; Murayama, K.; Takamuku, T.; Yamaguchi, T. *J. Phys. Chem.* **1995**, *99*, 462.
(9) Wakisaka, A.; Ohki, T. *Faraday Discuss.* **2005**, *129*, 231.
(10) Luck, W. A. P. *Ber. Bunsen-Ges. Phys. Chem.* **1963**, *67*, 186.
(11) Luck, W. A. P. *Ber. Bunsen-Ges. Phys. Chem.* **1965**, *69*, 626.
(12) Luck, W. A. P. *Angew. Chem., Int. Ed. Engl.* **1980**, *19*, 28.
(13) Suresh, S. J.; Naik, V. M. *J. Chem. Phys.* **2002**, *116*, 4212.
(14) Laaksonen, A.; Kusalik, P. G.; Svishchev, I. M. *J. Phys. Chem. A* **1997**, *101*, 5910.
(15) Dixit, S.; Crain, J.; Poon, W. C. K.; Finney, J. L.; Soper, A. K. *Nature* **2002**, *416*, 829.
(16) Dixit, S.; Soper, A. K.; Finney, J. L.; Crain, J. *Europhys. Lett.* **2002**, *59*, 377.
(17) Dougan, L.; Bates, S. P.; Hargreaves, R.; Fox, J. P. *J. Chem. Phys.* **2004**, *121*, 6456.
(18) Allison, S. K.; Fox, J. P.; Hargreaves, R.; Bates, S. P. *Phys. Rev. B* **2005**, *71*, 024201.
(19) Zhang, C.; Yang, X. *Fluid Phase Equilib.* **2005**, *231*, 1.
(20) Roney, A. B.; Space, B.; Castner, E. W.; Napoleon, R. L.; Moore, P. B. *J. Phys. Chem. B* **2004**, *108*, 7389.
(21) Fidler, J.; Rodger, P. M. *J. Phys. Chem. B* **1999**, *103*, 7695.
(22) Kusalik, P. G.; Lyubartsev, A. P.; Bergman, D. L.; Laaksonen, A. *J. Phys. Chem.* **2000**, *104*, 9533.
(23) Li, Z. X.; Lu, J. R.; Styrkas, D. A.; Thomas, R. K.; Rennie, A. R.; Penfold, J. *Mol. Phys.* **1993**, *80*, 925.
(24) Li., Z. X.; Lu, J. R.; Thomas, R. K.; Rennie, A. R.; Penfold, J. *J. Chem. Soc., Faraday Trans.* **1996**, *92*, 565.
(25) Sung, J.; Park, K.; Kim, D. *J. Phys. Chem. B* **2005**, *109*, 18507.
(26) Ju, S. S.; Wu, T. D.; Yeh, Y. L.; Wei, T. H.; Huang, J. Y.; Lin, S. H. *J. Chin. Chem. Soc.* **2001**, *48*, 625.
(27) Kataoka, S.; Cremer, P. S. *J. Am. Chem. Soc.* **2006**, *128*, 5516.
(28) Glinski, J.; Chavepeyer, G.; Platten, J. K. *J. Chem. Phys.* **1996**, *104*, 8816.
(29) Glinski, J.; Chavepeyer, G.; Platten, J. K.; Smet, P., *J. Chem. Phys.* **1998**, *109*, 5050.
(30) Matsumoto, M.; Takaoka, Y.; Kataoka, Y. *J. Chem. Phys.* **1993**, *98*, 1464.
(31) Tarek, M.; Tobias, D. J.; Klein, M. L. *J. Chem. Soc., Faraday Trans.* **1996**, *92*, 559; *Physica A* **1996**, *231*, 117.
(32) Stewart, E.; Shields, R. L.; Taylor, R. S. *J. Phys. Chem. B* **2003**, *107*, 2333.
(33) Andoh, Y.; Yasuoka, K. *Langmuir* **2005**, *21*, 10885.
(34) Jorgensen, W. L. *J. Phys. Chem.* **1986**, *90*, 1276.
(35) Berendsen, H. J. C.; Gigera, J. R.; Straatsma, T. P. *J. Phys. Chem.* **1987**, *91*, 6269.
(36) Allen, M. P.; Tildesley, D. J. *Computer Simulation of Liquids*; Oxford University Press: New York, 1987.
(37) Ryckart, J. P.; Ciccotti, G.; Berendsen, H. J. C. *J. Comput. Phys.* **1977**, *23*, 327.
(38) Berendsen, H. J. C.; Postma, J. P. M.; van Gunsteren, W. F.; Haak, J. R. *J. Chem. Phys.* **1984**, *81*, 3684.
(39) Susukita, R.; Ebisuzaki, T.; Elmegreen, B. G.; Furusawa, H.; Kato, K.; Kawai, A.; Kobayashi, Y.; Koishi, T.; McNiven, G. D.; Narumi, T.; Yasuoka, K. *Comput. Phys. Commun.* **2003**, *155*, 115.
(40) An additional *NVT* ($T = 298.15$ K) constant MD calculation was carried out where a 100 Å thick pure water layer was placed at the center of unit cell with the same dimension. The value of $\langle U_{ww} \rangle$ was calculated by the average of $U_{ww}(z)$ over bulk region of water layer.
(41) Gubskaya, A. V.; Kusalik, P. G. *J. Phys. Chem. A* **2004**, *108*, 7165.
(42) Haughney, M.; Ferrario, M.; McDonald, I. R. *J. Phys. Chem.* **1987**, *91*, 4934.
(43) Chowdhuri, S.; Chandra, A. *Phys. Rev. E* **2002**, *66*, 041203.
(44) Saiz, L.; Padro, J. A.; Guardia, E. *J. Phys. Chem. B* **1997**, *101*, 78.
(45) Chialvo, A. A.; Cumming, P. T. *J. Phys. Chem.* **1996**, *100*, 1309.
(46) Kirkwood, J. D.; Buff, F. P. *J. Chem. Phys.* **1951**, *19*, 774.
(47) Mountain, R. D. J. *J. Chem. Phys.* **1999**, *110*, 2109.
(48) Dellis, D.; Chalaris, M.; Samios, J. *J. Phys. Chem. B* **2005**, *109*, 18575.
(49) McQuarrie, D. A.; Simon, J. D. *Physical Chemistry: A Molecular Approach*; University Science Books: Sausalito, CA, 1997.